Probing the limitations of Sigmund's model of spatially resolved sputtering using Monte Carlo simulations

Gerhard Hobler, R. Mark Bradley, and Herbert M. Urbassek

Phys. Rev. B **93**, 205443 — Published 31 May 2016

DOI: 10.1103/PhysRevB.93.205443

Probing the limitations of Sigmund's model of spatially resolved sputtering using Monte Carlo simulations

Gerhard Hobler,[1] R. Mark Bradley,[2] and Herbert M. Urbassek[3]

[1]*Institute of Solid-State Electronics, TU Wien, Floragasse 7, A-1040 Wien, Austria*
[2]*Department of Physics, Colorado State University, Fort Collins, Colorado 80523, USA*
[3]*Physics Department and Research Center OPTIMAS, University Kaiserslautern, Erwin-Schrödinger-Straße, D-67663, Germany*

(Dated: March 9, 2016)

Sigmund's model of spatially resolved sputtering is the underpinning of many models of nanoscale pattern formation induced by ion bombardment. It is based on three assumptions: (i) the number of sputtered atoms is proportional to the nuclear energy deposition (NED) near the surface, (ii) the NED distribution is independent of the orientation and shape of the solid surface and is identical to the one in an infinite medium, and (iii) the NED distribution in an infinite medium can be approximated by a Gaussian. We test the validity of these assumptions using Monte Carlo simulations of He, Ar, and Xe impacts on Si at energies of 2, 20, and 200 keV with incidence angles from perpendicular to grazing. We find that for the more commonly-employed beam parameters (Ar and Xe ions at 2 and 20 keV and non-grazing incidence), the Sigmund model's predictions are within a factor of 2 of the Monte Carlo results for the total sputter yield and the first two moments of the spatially resolved sputter yield. This is partly due to a compensation of errors introduced by assumptions (i) and (ii). The Sigmund model, however, does not describe the skewness of the spatially resolved sputter yield, which is almost always significant. The approximation is much poorer for He ions and/or high energies (200 keV). All three of Sigmund's assumptions break down at grazing incidence angles. In all cases, we discuss the origin of the deviations from Sigmund's model.

PACS numbers: 81.16.Rf, 79.20.Ap, 79.20.Rf
Keywords: sputtering, pattern formation, Monte Carlo simulations

I. INTRODUCTION

Bombarding a solid surface with a broad ion beam can produce a remarkable variety of self-assembled nanoscale patterns [1], including periodic height modulations [2] and mounds arranged in hexagonal arrays of surprising regularity [3, 4]. The spontaneous emergence of these patterns is not just fascinating in its own right, since there is widespread interest in using ion bombardment to fabricate nanostructures.

The underpinning of many models of nanoscale pattern formation induced by ion bombardment is the Sigmund model of spatially resolved sputtering [5]. The Bradley-Harper (BH) theory, for example, provides one possible explanation for why oblique-incidence ion bombardment often produces ripples on solid surfaces [6]. In that theory, a partial differential equation is derived which gives the time evolution of the solid surface due to the combined effects of sputtering and surface diffusion; the theory applies to long wavelength disturbances at sufficient early times. The Sigmund model is used to model the effects of sputtering in the BH theory. Since the BH theory was introduced in 1988, many extensions of the theory have been developed in which its limitations are to some extent surmounted [7–14]. All of these theories are based on the Sigmund model.

The Sigmund model is approximate, but it is also analytically tractable. Bradley and Harper were able to explicitly compute the coefficients in the continuum equation of motion thanks to its relatively simple form. The model also allows us to gain an intuitive understanding of how it is that a planar surface can be destabilized by ion sputtering and of why nanoscale patterns form. In recent years it has become clear that momentum transfer from the incident ions can induce mass currents in the near surface region, and that these currents can play a key role in the surface dynamics [8, 12, 15–18]. However, sputtering likely has a crucial influence on the pattern formation for many choices of ion beam and target material, particularly for ion energies in excess of 1 keV.

The Sigmund model continues to be important in the theoretical development of the field. Recently, there has been considerable interest in incorporating the results of molecular dynamics (MD) or Monte Carlo (MC) simulations into a continuum theory of ion-induced surface dynamics. The so-called crater function formalism utilizes the average result of many ion impacts at a single point to generate a crater function, which is then used to determine the response of a surface to bombardment with a broad ion beam [19, 20]. The formalism yields estimates of the constant coefficients that appear in the continuum equation of motion based on input from simulations. Harrison and Bradley extended the crater function formalism used in Ref. [20] so that it included the effect of the curvature dependence of the crater function [21]. They then tested their formalism by applying it to Sigmund's model of ion sputtering and found that it indeed reproduced the exact BH curvature coefficients.

For a flat surface, the Sigmund model gives a sputter yield that is an increasing function of the angle of in-

cidence θ for all values of θ between zero and 90°. In contrast, experiments invariably show that the sputter yield at first increases with θ, but then attains a maximum before falling to zero at grazing incidence. It is therefore remarkable that the Sigmund model does quite well in predicting how the sputter yield depends on the surface curvature if the angle of incidence is not too close to grazing and the radii of curvature are not too small [22, 23].

In Sigmund's model **as it is applied to ion-induced pattern formation** [5], it is assumed that

(i) the number of sputtered atoms is proportional to nuclear energy deposition (NED) near the surface,

(ii) the NED distribution is independent of the orientation and shape of the surface and is identical to the one in an infinite medium, and

(iii) the NED distribution in an infinite medium can be approximated by a Gaussian.

For the sake of historical correctness, we mention that assumption (i) is actually a result of Sigmund's earlier work [24], which followed from more fundamental assumptions like that of an isotropic homogeneous medium. In particular, his result is valid asymptotically in the limit that the impact energy, which defines the spatial scale of the cascade, is large compared to the surface binding energy, which governs sputtering. For the purpose of this paper we refer to (i) as Sigmund's assumption (i).

Surprisingly, in spite of the model's 40+ years of use, there is a lack of thorough assessments of these assumptions. As a notable exception, Hossain et al. [25], using MD simulations of low-energy ion impacts, recently found assumption (i) to be violated, while their data confirmed assumption (iii). The current paper provides a more comprehensive study.

NED is energy loss from a collision cascade due to elastic collisions with the target nuclei. In a binary collision framework, it is comprised of energy transferred to target atoms that are not displaced from their sites (subthreshold collisions), the binding energies of target atoms that recoil from their sites, and the remaining energies of the ion and the recoils when their trajectories are terminated. NED is sometimes thought of being converted into lattice vibrations, therefore it is referred to as "phonons" in the popular SRIM simulation code [26]. However, nuclear energy deposition may also be converted into potential energy associated with lattice disorder, i.e. defect formation or amorphization. We therefore prefer the term NED.

The meaning of NED in an MD context is less well defined, since in MD all atoms move and the distinction between recoils and lattice atoms having received "nuclear energy" is ambiguous. A viable concept has been proposed [25] that determines the total energy at a time when the recoils have lost most of their energy, but before the energy has spread by heat conduction. It is not completely clear, however, to what extent this technique is equivalent to the traditional definition of NED in the binary collision picture. For this reason and to allow a much larger number of simulations at higher energies, we have chosen Monte Carlo (MC) binary collision simulations as the vehicle for our tests.

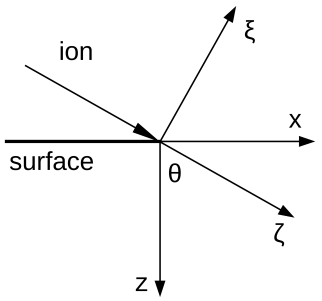

Figure 1: The coordinate system (ξ, η, ζ) has the ζ axis parallel to the incidence direction. The ξ axis is within the plane of the incidence direction and its projection onto the surface. The coordinate system (x, y, z) has its x axis along the surface, the z axis perpendicular to the surface, and $y = \eta$. θ denotes the incidence angle.

Before presenting our investigation, a few words on Sigmund's assumptions (i)–(iii) seem appropriate. Assumption (i) is equivalent to demanding that the sputtering efficiency Λ is a constant, where Λ is defined by

$$\mathrm{d}Y(x,y) = \Lambda(x,y)\, F(x,y,z)\, \mathrm{d}A. \qquad (1)$$

Here, $F(x,y,z)$ denotes the NED density [eV/Å^3] per incident ion, $\mathrm{d}A$ the area of a chosen element at the surface $z = z(x,y)$ from which atoms are sputtered, and $\mathrm{d}Y(x,y)$ the local sputter yield, i.e. the number of atoms sputtered from the surface element per incident ion. We note that Eq. (1) is the definition of Λ Sigmund used in his original work [5], while later work which focused on the surface velocity rather than the sputter yield included the target density in the definition of Λ [6].

Assumption (i) says that $\Lambda(x,y)$ is a constant for a given target material and "state of the surface", which includes surface crystallinity, orientation, and defects [5, 24]. In particular, Λ is assumed to be independent of the surface position (x,y) and the beam parameters. It has turned out, however, that Λ is a function of ion species and incidence energy [27]. This implies that it is also a function of surface position, since an ion with incidence energy E_0 is slowed down to energies below E_0 while traveling into the target. The lower energies dominate towards the periphery of the collision cascade, and so if Λ depends on E_0, then it should also depend on the position within the cascade.

Assumption (ii) says that the NED distribution $F(x,y,z)$ can be obtained at any incidence angle θ and for any surface shape from the NED distribution in an

infinite medium $F_\infty(\xi,\eta,\zeta)$. In particular,

$$F(x,y,z) = F_\infty(\xi,\eta,\zeta), \tag{2}$$

where ξ, η and ζ are obtained from x, y and z by a rotation about the y axis through the incidence angle θ:

$$\begin{aligned} \xi &= x\cos\theta - z\sin\theta \\ \eta &= y \\ \zeta &= x\sin\theta + z\cos\theta. \end{aligned} \tag{3}$$

Here we have assumed that the impact point is at the origin of both the (x,y,z) and the (ξ,η,ζ) coordinate system, that the ζ axis is aligned with the beam direction, and that the y and η axes coincide (see Fig. 1).

There are several effects leading to deviations from assumption (ii) [28]. The most intuitive is the "absorption" of particles **(ions or recoils)** by the surface. In the case of a planar surface, this occurs because particles that have left the target cannot reenter it **and cannot generate cascades of recoils that reenter. Sigmund has derived a relation between F and F_∞ at the real and imaginary surface, respectively [51], which in our notation and rearranged to give the ratio F/F_∞, reads**

$$\frac{F}{F_\infty} = \frac{1 - r\langle F_\infty\rangle/F_\infty}{1 + \Lambda\langle F_{\infty,\mathrm{r}}\rangle}. \tag{4}$$

Here r denotes the reflection coefficient of the ions and $F_{\infty,\mathrm{r}}$ the energy deposition function of a recoil in an infinite medium. The averages $\langle\ \rangle$ run over the angular and energy spectra of the sputtered atoms and reflected ions at the surface. The NED ratio F/F_∞ equals unity if assumption (ii) is fulfilled. F/F_∞ as determined from Monte Carlo simulations will serve us to evaluate the validity of assumption (ii). Eq. (4) qualitatively shows that both ion reflection and recoils leaving the target decrease NED at the surface compared to NED at an imaginary surface in an infinite medium. The averages in Eq. (4), however, have proven to be difficult to evaluate, and so no analytical model exists for the reduction of NED by the surface. The situation is even more complicated at non-planar surfaces as the absorption effect depends on the shape of the surface between the impact point and the point of sputtering.

We note that assumption (i) is usually written as $Y = \Lambda F_\infty$ rather than $Y = \Lambda F$. This makes no difference as long as assumption (ii) is fulfilled, which is almost always assumed. We prefer the definition of Λ given by Eq. (1), since we consider it more physical to define this quantity in terms of other quantities that describe the same semi-infinite target. This definition is also in accord with Sigmund's assertion that the energy deposition function should be calculated "preferably by dropping the assumption of an infinite target" [24].

The Gaussian approximation (assumption (iii)) says that $F_\infty(\xi,\eta,\zeta) = F_\mathrm{G}(\xi,\eta,\zeta)$ with

$$F_\mathrm{G}(\xi,\eta,\zeta) = \frac{\varepsilon}{(2\pi)^{3/2}\alpha\beta^2}\exp\left(-\frac{(\zeta-a)^2}{2\alpha^2} - \frac{\xi^2+\eta^2}{2\beta^2}\right). \tag{5}$$

The parameters a, α, and β denote the mean depth and the longitudinal and lateral standard deviations, respectively, of the NED density, while ε is the energy deposited in nuclear collisions per incident ion, i.e., the energy of the incident ion minus the energy lost in electronic processes. Note that because of assumption (ii) these parameters do not depend on the incidence angle or the surface shape. Assumption (iii) is not intrinsic to Sigmund's model. In fact, Sigmund explored several more refined approximations to the 1D NED distribution [24]. However, he later stated that "the Gaussian approximation has been found to be sufficient in most situations discussed in connection with calculations of the sputtering yield" [5]. On the other hand, more refined approximations have not been used to describe non-local effects in sputtering. More sophisticated functions such as those employed in the modeling of implanted dopant distributions in semiconductors [29] would be difficult to use in pattern formation theories. We therefore consider the Gaussian approximation to be an integral part of Sigmund's model for the purposes of this study.

In the following, after describing our Monte Carlo method, we investigate the validity of assumptions (i)–(iii) in sequence, and then study the combined effect of all assumptions. We restrict ourselves to Si targets, since it is a common material used in technology, it amorphizes under ion bombardment so that channeling effects are largely avoided, and it is of medium mass so that both ions lighter and heavier than the target can be studied. We also limit the scope of this study to planar surfaces. We investigate the ion mass dependence by considering He, Ar, and Xe ions, and the energy range from 2 to 200 keV. Sputtering of Si by Ar and Xe has frequently been studied in the literature. Sputtering by He beams has recently received interest due to the introduction of the helium ion microscope [30].

II. MONTE CARLO SIMULATION MODEL

All MC simulations are performed with the IMSIL code in its static mode [31, 32]. Special attention is paid to obtaining consistent and accurate sputter yields and NED distributions. For the former the usual assumption is made that sputtered atoms, before leaving the target, travel through a planar potential barrier [24, 33] whose height is the surface binding energy E_s. We use a value of 4.7 eV corresponding to the heat of sublimation of Si. For the calculation of NED we consider the energy transferred in subthreshold collisions and the remaining energy of stopped atoms; bulk binding energies are neglected in the simulation of the collision cascade and therefore also

in the calculation of NED. The total amount of NED is mainly determined by the ratio of nuclear to electronic stopping power. We use the ZBL potential as the interatomic potential and a mixed Lindhard/Oen-Robinson model for electronic stopping with an equipartition rule. In addition, NED depends on three model parameters in a more subtle way: The displacement energy E_d determines which recoils are followed. Since the energy of atoms that are not followed is counted entirely as NED, any electronic energy loss along the remaining path is neglected. Similarly, the cutoff-energy E_f for trajectories determines when a trajectory is terminated and any electronic stopping below E_f is neglected. The third parameter influencing NED is the maximum impact parameter p_max, which introduces a lower limit for energy transfers taken into account by the simulation. Ideally, $E_\mathrm{d} \to 0$, $E_\mathrm{f} \to 0$, $p_\mathrm{max} \to \infty$ would give us the amount of NED consistent with the nuclear and electronic stopping models. In practice, finite values have to be used. We choose $E_\mathrm{d} = E_\mathrm{f} = E_\mathrm{s}$, since E_s is an upper limit for E_d and E_f in the vicinity of the surface in order to obain correct sputter yields. $E_\mathrm{d} = E_\mathrm{s}$ will overestimate the number of Frenkel pairs in the bulk, but we are not interested in that quantity here. Effectively, $E_\mathrm{d} = E_\mathrm{f} = E_\mathrm{s}$ means that the range and electronic stopping of atoms with energy less than E_s are neglected.

The target material is assumed to be amorphous, and so the collision partners are selected randomly. The free flight paths are chosen with an exponential probability density [34] and a mean value determined by the target density and p_max [35]. In IMSIL, the maximum impact parameter p_max and consequently the mean free flight paths are taken to depend on the energy in such a way that all nuclear energy transfers down to a specified threshold are considered [36]. Since we are interested in accurate NED distributions, we use a low value of 0.1 eV for the minimum nuclear energy transfer and impose an additional upper limit of 4 Å to p_max. The time integral is neglected as well as the influence of local electronic stopping on scattering angles. In all simulations cascades of 100000 impinging ions are simulated, except for He ions, where 1 million He ions are used.

At glancing incidence angles the treatment of collisions before the ion enters the target is essential. In IMSIL the ions start at a distance p_max outside the target **such that their undeflected direction of motion goes through the origin**. Positions of potential collision partners are determined in the usual way, but target atoms are generated at these positions only if they are inside the user-defined surface [35]. Such an algorithm is most likely not applied in SRIM which might account for its failure to correctly predict glancing angle sputter yields [37].

In IMSIL it is possible to start the ions in the interior of the target. This mode is used to run reference simulations to study the influence of the surface on the NED distribution**, and to determine the parameters for the Gaussian approximation**. These simulations are referred to as "infinite-medium" simulations as opposed to simulations in "semi-infinite" targets that use a planar surface.

For the calculation of spatially resolved sputter yields the positions where sputtered recoils originate from [27] are recorded as a histogram. For the calculation of spatially resolved surface NED, multi-dimensional histograms are recorded, and the surface NED is extrapolated from the two histogram boxes closest to the surface.

Sigmund's theory requires the parameters a, α, β, and ε. To test our code, we have compared the values of these parameters**, obtained under semi-infinite target conditions,** for 20 keV Ar in Si with the values obtained with other codes (Table I). Excellent agreement between IMSIL and TRI3DST as reported by Nietiadi et al. [38] and reasonable agreement with SRIM-2013 [39] is observed, while results obtained with a modified version of SDTrimSP [27] differ significantly. The SRIM-2013 values have been obtained from the depth distribution of "phonons". SRIM-2013 has a different electronic stopping power model. Both the smaller range parameters and the lower total NED as compared to our simulations are consistent with a larger electronic stopping power in SRIM. The larger deviation of the SDTrimSP results may also be due to a different electronic stopping model and to a different method of extracting the parameters: In [27] a Gaussian was fitted to the NED distribution, while in IMSIL the parameters are calculated by accumulating the statistical moments of NED during the MC simulation.

Excellent agreement between IMSIL and TRI3DST is also found in the 2D NED distributions, both for normal incidence ($\theta = 0°$, Fig. 2(a)) and at an incidence angle of $\theta = 70°$ (Fig. 2(b)). For these plots both distributions are scaled with their respective total NEDs. The excellent agreement between IMSIL and TRI3DST, two independently developed codes, gives confidence in the validity of our simulations.

III. SPUTTERING EFFICIENCIES

Sigmund's first assumption is the proportionality between sputter yield and NED close to the surface. If valid, sputtering efficiencies (defined as the ratio of sputter yield to the NED) should be constants depending ex-

	IMSIL this work	TRI3DST [38]	SRIM-2013 [39]	SDTrimSP [27]
a [Å]	206.4	208.9	200.2	149
α [Å]	121.3	123.0	111.9	114
β [Å]	77.7	79.7		47
ε [keV]	11.9		10.7	

Table I: NED moments for 20 keV Ar in Si as obtained from different MC simulation codes: mean NED depth a, longitudinal standard deviation α, lateral standard deviation β; and total NED ε.

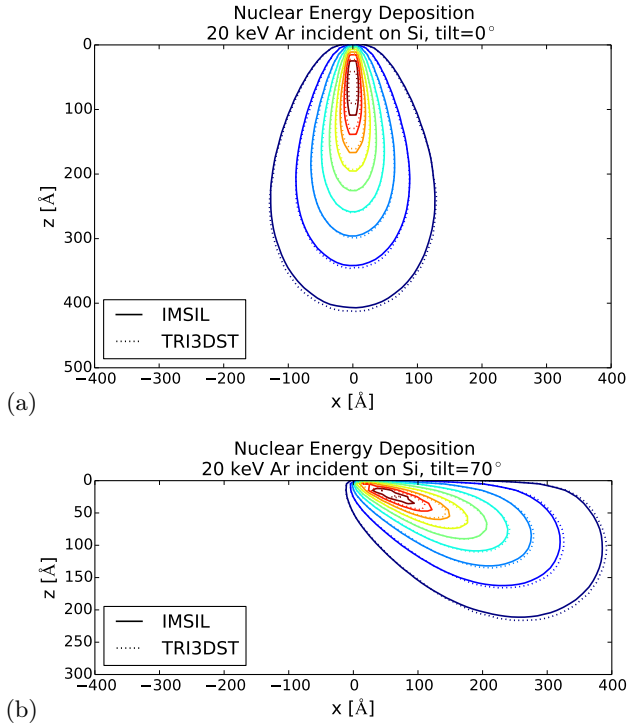

Figure 2: NED distributions for 20 keV Ar in Si as calculated with IMSIL (solid lines) and TRI3DST [38] (dotted lines) for (a) normal incidence and (b) an incidence angle of 70°. The distributions have been scaled to the same total NED. The levels correspond to 10% (dark blue lines), 20% (blue), ... 90% (dark red) of the maximum Monte Carlo energy density.

clusively on the target material. We test this assumption by calculating the sputtering efficiency as obtained from MC simulations for a planar surface ($z(x,y)=0$) as a function of surface position and ion beam parameters (incidence angle, mass, and energy of the ion).

A. Spatial Dependence

We could calculate the sputtering efficiency $\Lambda(x,y)$ with IMSIL using Eq. (1). However, to simplify the graphical representation of the results, we report the average of $\Lambda(x,y)$ along the y direction weighted with the NED distribution $F(x,y,z=0)$,

$$\bar{\Lambda}(x) = \int \Lambda(x,y)\, F(x,y,z=0)\, \mathrm{d}y \Big/ \int F(x,y,z=0)\, \mathrm{d}y. \tag{6}$$

The denominator of the right-hand side of Eq. (6) is the 2D NED distribution

$$F_{2\mathrm{D}}(x,z) = \int F(x,y,z)\, \mathrm{d}y \tag{7}$$

(which has the units [eV/Å^2]) evaluated at the surface. Inserting ΛF from Eq. (1) in Eq. (6), it is easily seen that the numerator is equal to the differential sputter yield $\mathrm{d}Y/\mathrm{d}x$ ($= \int \mathrm{d}Y/\mathrm{d}A\, \mathrm{d}y$). Thus,

$$\bar{\Lambda}(x) = \frac{\mathrm{d}Y}{\mathrm{d}x}(x) \Big/ F_{2\mathrm{D}}(x, z=0). \tag{8}$$

Both $\mathrm{d}Y/\mathrm{d}x(x)$ and $F_{2\mathrm{D}}(x,z)$ have been calculated with IMSIL as histograms. We have also calculated forward sputter yields from membranes with thickness equal to the mean NED depth a. In this case the sputtering efficiency is obtained by replacing $F_{2\mathrm{D}}(x, z=0)$ with $F_{2\mathrm{D}}(x, z=a)$ in Eq. (8).

The results for 20 keV Ar bombardment of Si at normal incidence are shown in Figs. 3(a) and (b). In both backward (Fig. 3(a)) and forward sputtering (Fig. 3(b)), the sputtering efficiency is roughly 0.2 Å/eV; however, in the case of backward sputtering the sputtering efficiency dips around the impact point, while it peaks there for forward sputtering. More dramatic variations of the sputtering efficiency are observed, e.g., for normally incident 2 keV Xe ions and for **the extreme case of** 20 keV He ions at a glancing incidence angle of 80° (Figs. 3(c) and (d), respectively).

B. Dependence on Ion Beam Parameters

To condense the data further, we have taken the weighted averages of the sputtering efficiency $\bar{\Lambda}(x)$ over the x direction to yield

$$\bar{\bar{\Lambda}} = \int \bar{\Lambda}(x)\, F_{2\mathrm{D}}(x, z=0)\, \mathrm{d}x \Big/ \int F_{2\mathrm{D}}(x, z=0)\, \mathrm{d}x. \tag{9}$$

Inserting Eq. (8) in Eq. (9), using $Y = \int \mathrm{d}Y/\mathrm{d}x\, \mathrm{d}x$, and defining the 1D NED distribution

$$F_{1\mathrm{D}}(z) = \int F_{2\mathrm{D}}(x,z)\, \mathrm{d}x \tag{10}$$

(which has the units [eV/Å]), we obtain the average sputtering efficiency

$$\bar{\bar{\Lambda}} = Y / F_{1\mathrm{D}}(z=0). \tag{11}$$

Both Y and $F_{1\mathrm{D}}(z)$ have been calculated with IMSIL. The forward sputtering efficiency is obtained by replacing $F_{1\mathrm{D}}(z=0)$ with $F_{1\mathrm{D}}(z=a)$ in Eq. (11).

Backward and forward sputtering efficiencies $\bar{\bar{\Lambda}}$ are shown as a function of incidence angle in Figs. 4(a) and (b), respectively. Data are shown for He, Ar, and Xe ions with energies of 2, 20, and 200 keV. All backward sputtering efficiencies increase moderately as a function of incidence angle up to about 70°. The sputtering efficiencies for the lower energies and/or higher masses pass through a maximum and decrease rapidly at glancing angles, while those of the light, high energy ions keep increasing at glancing incidence angles. In contrast to the backward sputtering efficiencies, the forward sputtering

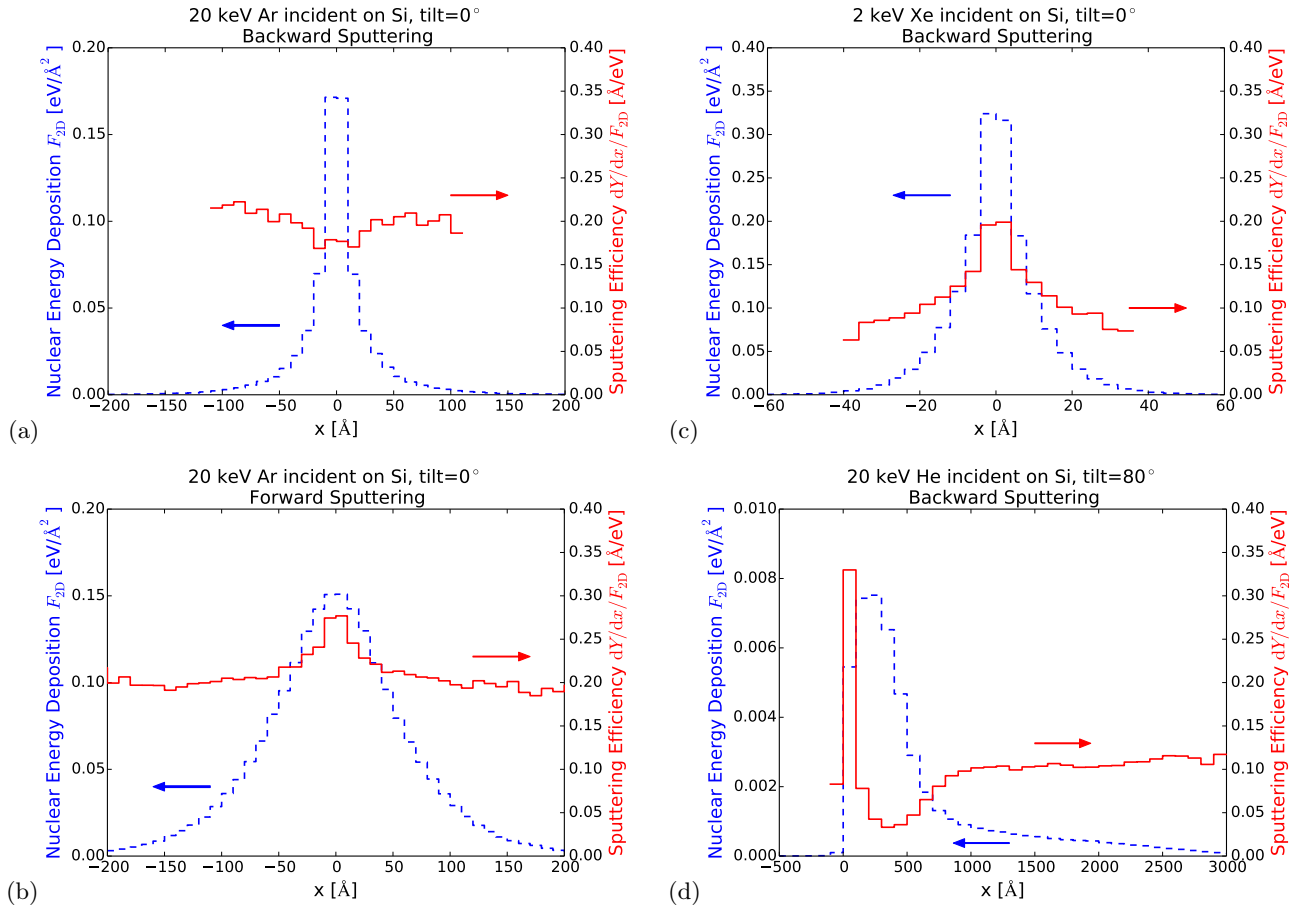

Figure 3: Surface NED densities $F_{2D}(x, z)$ (blue dashed histograms) and space dependent sputtering efficiencies $\bar{\Lambda}(x) = dY/dx/F_{2D}(x, z)$ (Eq. (8), red solid histograms) along the surface for 20 keV Ar at normal incidence and (a) backward sputtering from a semi-infinite target, (b) forward sputtering from a membrane of thickness 200 Å ($\approx a$), (c) for 2 keV Xe at normal incidence, and (d) 20 keV He at an incidence angle of 80° for a semi-infinite target.

efficiencies exhibit only a weak dependence on the angle of incidence.

Figure 4 suggests that the ion mass and energy dependencies are actually more pronounced than the incidence angle dependence, except at angles very close to grazing incidence. In Figs. 5(a) and (b) the sputtering efficiencies at normal incidence are replotted as a function of ion species and incidence energy, respectively. As a general trend, the sputtering efficiency increases with ion mass, while the trend with respect to incidence energy is less clear. The backward and forward sputtering efficiencies behave similarly in these plots, with forward sputtering always being more efficient than backward sputtering. The difference between the forward and backward sputtering efficiencies increases with decreasing energy. Note that the efficiencies for backward sputtering by 200 keV He ions and forward sputtering by 20 keV Xe ions differ by a factor of 5. The sputtering efficiencies for more common beam parameters (Ar and Xe ions at 2 and 20 keV), however, are within a factor of 2 of one another.

C. Discussion

Our results on the parameter dependence of the sputtering efficiency presented in the previous subsections can be understood by considering the energy spectrum of the recoils and by directional effects. Since the recoils must surmount the surface binding energy to be sputtered, a larger fraction of recoils with energies above the surface binding energy will lead to a higher sputtering efficiency. Likewise, a greater tendency for recoils to move towards the surface will increase the sputtering efficiency.

Considering the energy spectrum of the recoils explains the ion mass dependence seen in Fig. 5(a): As quantified in Fig. 6, heavier ions produce more energetic recoils with a higher fraction of them above the surface binding energy. A more subtle argument is required to see why forward sputtering efficiencies are higher than their backward counterparts, as seen in Fig. 5. Basic collision kinetics dictates that recoils with higher energy have a larger initial component in the direction of the projectile [40]. This causes recoils reaching the forward surface to have higher kinetic energies on average than those reach-

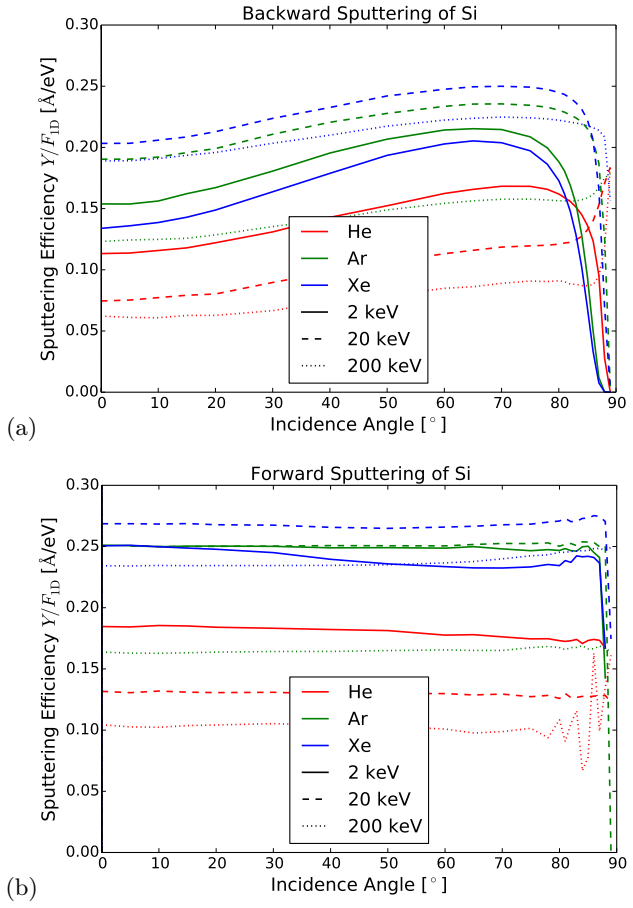

Figure 4: (a) Backward and (b) forward sputtering efficiencies $\bar{\bar{\Lambda}} = Y/F_{1D}$ as a function of incidence angle for He, Ar, and Xe ions with energies of 2, 20, and 200 keV.

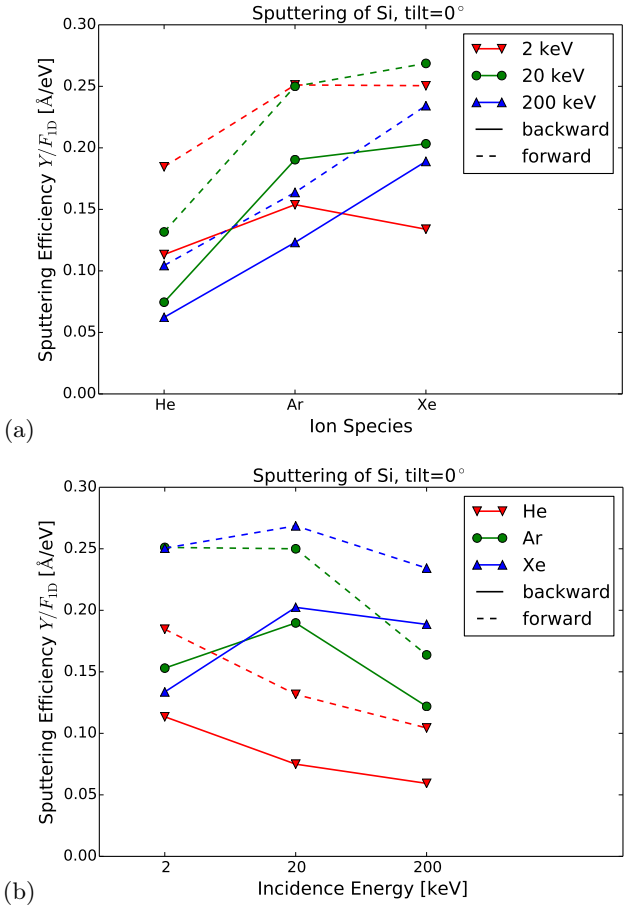

Figure 5: (a) Ion mass and (b) incidence energy dependence of the sputtering efficiency $\bar{\bar{\Lambda}} = Y/F_{1D}$ at normal incidence.

ing the backward surface. For example, IMSIL simulations yield average energies of forward and backward sputtered atoms of 525 eV and 70 eV, respectively, for 20 keV Ar ions. Once again, higher recoil energies lead to higher sputtering efficiency.

Collision kinetics also dictates that recoils must have a positive momentum component in the direction of the projectile. Thus, when the ion is normally incident on a planar surface, the primary recoil cannot be sputtered directly. Instead, for the primary recoil to be sputtered, it must experience another collision and this collision must send it toward the solid surface. The primary recoil can also collide with another atom in such a way that the latter recoils toward the surface (Fig. 7, left). In both cases the energy of the recoil moving toward the surface is less than the initial energy of the primary recoil, and the probability for sputtering is reduced. Therefore, there is a tendency for backward sputtering to be reduced at normal incidence. When the incidence angle is increased, direct sputtering of primary recoils becomes possible (Fig. 7, right), which increases the sputtering efficiency. A clear signature of this direct sputtering is seen in Fig. 3(d) (20 keV He at 80°) in the sharp peak of the

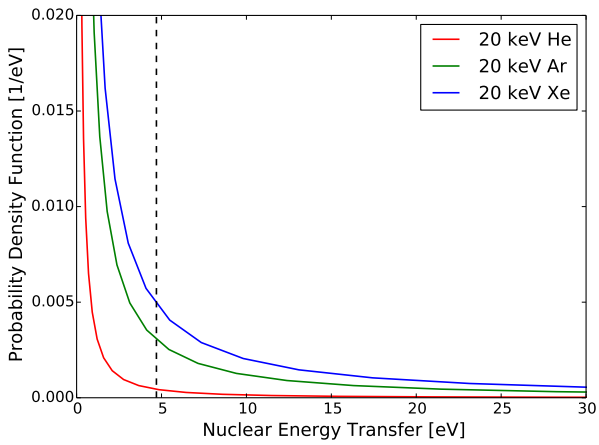

Figure 6: Energy spectra of recoils from 20 keV He, Ar, and Xe ions in amorphous Si calculated using the universal ZBL potential. Note there is a sharp peak at very small energies (not shown) which compensates for the apparently different areas below the curves. The dashed line indicates the surface binding energy of Si.

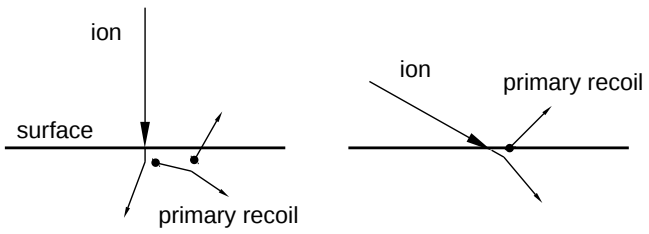

Figure 7: Sketch illustrating the impossibility of the first primary recoil being sputtered without further interaction with the target when the ion is normally incident on the surface (left). For oblique incidence, direct sputtering of primary recoils is possible (right).

sputtering efficiency close to the impact point. This effect increases with increasing incidence angle, which explains the increase in backward sputtering efficiency with incidence angle (Fig. 4(a)). **Sigmund's theory of sputtering fails to describe these effects, since it is assumed in the theory that the recoils generated near the surface have a certain energy distribution ($\sim E^{-2}$) and an isotropic angular distribution [28]. These conditions are typically not fulfilled for primary recoils generated by the ions in the early parts of their trajectories.**

It is also interesting to observe that backward sputtering efficiencies decrease as a function of incidence angle for near-grazing incidence of low-energy ions (solid lines in Fig. 4(a)). A possible explanation for this is that a large fraction of these ions does not penetrate into the target at all. When ions are reflected from the surface, they deposit energy in the top layer of the target, but only generate recoils that move into the target. These recoils cause collision cascades that have a low probability of extending back to the surface with recoils of sufficient energy to produce sputtering. Thus, the surface leads to ion trajectories and NED that differ markedly from those in an isotropic medium.

Directional effects may also be discussed in terms of the anisotropy of the collision cascade. Sckerl et al. used transport theory to investigate the angular distribution of recoils in a collision cascade as a function of recoil energy [41–43]. One of the findings of that work is that cascade anisotropy, defined as the recoil flux density divided by its isotropic component, decreases as the ratio of the recoil energy under consideration and the impact energy decreases. This finding provides further support for our observation of larger forward than backward sputtering efficiencies: For energetic recoils, anisotropy is still very pronounced: Downstream from the ion impact point, energetic recoils fly preferentially in the ion impact direction, while at the bombarded surface – due to the difficulty of momentum reversal – they reach the surface at more oblique angles. Low-energy recoils move more isotropically, and have a larger probability of reaching the backward surface. Therefore, the ratio of energetic to low-energy recoils is larger at the forward than at the backward surface. Sckerl at al.'s finding also explains why the difference between forward and backward sputtering is larger at low incidence energies (cf. Fig. 5(b)): The relevant recoil energy for sputtering is the surface binding energy, which is independent of the impact energy; at lower impact energies the ratio of surface binding energy and impact energy is larger, and therefore the cascade is more anisotropic.

IV. INFLUENCE OF THE SURFACE

We recall that the presence of a surface leads to a reduction of NED due to the "absorption" of ions and recoils by the surface, since ions and recoils cannot be scattered back into the target once they have left it [28]. In this section, we investigate the magnitude of this effect under various conditions by comparing NED in the presence of a surface with NED in the infinite medium. Stated more precisely, we compare $F_{2\mathrm{D}}(x,z)$ and $F_{1\mathrm{D}}(z)$ with their analogues for the infinite medium, $F_{2\mathrm{D},\infty}(x,z)$ and $F_{1\mathrm{D},\infty}(z)$. As in Section III, we restrict ourselves to the 1D and 2D NED distributions to simplify the graphical representation.

A. Spatial dependence

In Fig. 8 the NED distribution in an infinite medium is compared with that of a membrane with a thickness of 200 Å for 20 keV Ar incident on Si. Unsurprisingly, the membrane NED is mostly restricted to the interval [0,200] Å. The small tails visible outside this layer are due to adatoms, i.e., recoil atoms stopped between the target and the plane of the potential well used to implement the surface binding energy. As expected, NED is reduced close to the surfaces. For normal incidence (Fig. 8(a)), the reduction in NED is much stronger at the forward surface (∼50%) than at the backward surface (∼10%). For glancing incidence ($\theta = 85°$, Fig. 8(b)), the effect is large across the whole membrane, including at the backward surface. This is because in this case the reflection coefficient of $r = 0.61$ is significant in the membrane simulation, and the energy carried away by the reflected ions cannot be deposited. In contrast, in the infinite-medium simulation, projectiles scattered into the $z < 0$ half-space may return to the "target", i.e. the region $z > 0$. Recoils generated by projectiles entering the region $z < 0$ may also enter the region $z > 0$.

In Fig. 8(b), the green dotted line represents the NED distribution for an infinite medium multiplied by $1 - r$, which implements the assumptions that the reflected ions carry away all of their incident energy and therefore cause no NED in the target, while NED from recoil cascades of ions that are not reflected are unaffected by the surface. In reality, both contributions are finite. The en-

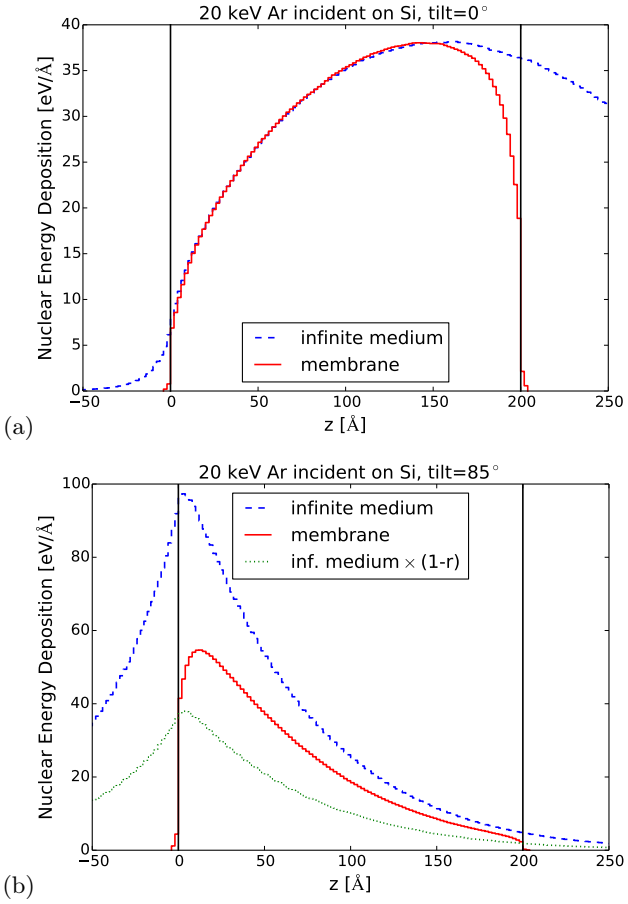

Figure 8: NED densities as a function of depth in an infinite medium ($F_{1D,\infty}(z)$, blue dashed lines) and in a membrane ($F_{1D}(z)$, red solid lines) for 20 keV Ar in Si (a) at normal incidence and (b) at an incidence angle of 85°. The surfaces are indicated by the vertical black lines. The green dotted line refers to a model that neglects all NED from backscattered ions and the influence of the surface on recoils from unreflected ions.

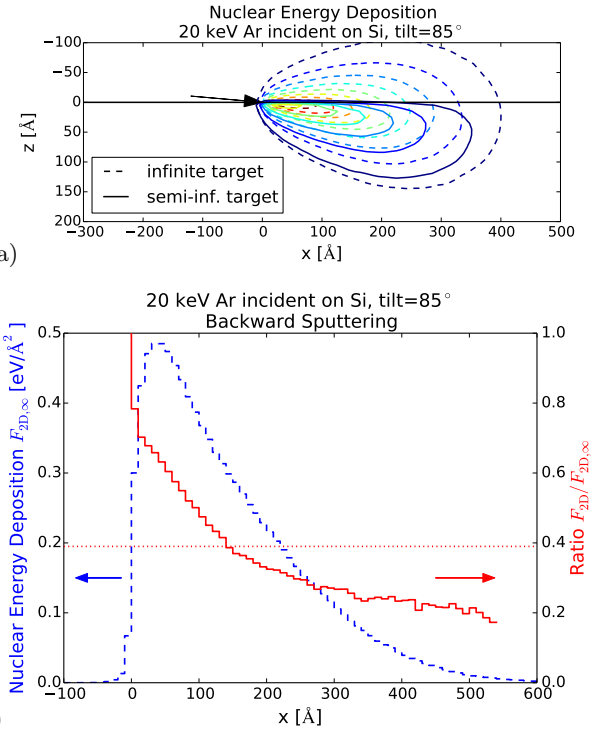

Figure 9: (a) 2D NED distributions for 20 keV Ar incident on Si at an angle of 85°. The distribution for a semi-infinite target $F_{2D}(x,z)$ (solid lines) and the distribution for an infinite medium $F_{2D,\infty}(x,z)$ (dashed lines). The levels correspond to 10% (dark blue lines), 20% (blue), ... 90% (dark red) of the maximum NED in the infinite medium. (b) NED distribution $F_{2D,\infty}(x,z=0)$ and the ratio $F_{2D}(x,z=0)/F_{2D,\infty}(x,z=0)$ along the surface.

ergy transfer from the reflected ions to the target leads to larger NED, while absorption of recoils generated by unreflected ions reduces NED. From Fig. 8(b) it may be seen that the positive effect on NED is quite significant and reaches deep into the target, i.e., recoil cascades of reflected ions are important and spatially quite extended. The negative effect of surface absorption of recoils generated by unreflected ions appears to be responsible for the smaller difference between the membrane simulation (red line) and the modified infinite medium simulation (green line) close to the surfaces. This will be further discussed in Section IV C. The reasonable agreement between the surface values of the red and green line is due to the compensation of the two effects and seems to be fortuitous.

Figure 9(a) shows the 2D NED distributions for the semi-infinite and infinite mediums for the same bombardment conditions as in Fig. 8(b). The most prominent differences between infinite-medium and semi-infinite-target simulations are found close to the surface. In Fig. 9(b) the NED distribution $F_{2D,\infty}(x,z=0)$ and the ratio $F_{2D}(x,z=0)/F_{2D,\infty}(x,z=0)$ are plotted versus the surface position x. The ratio $F_{2D}/F_{2D,\infty}$ is considerably less than unity, which illustrates the significant influence of the surface on NED. The decrease of $F_{2D}/F_{2D,\infty}$ as a function of x reveals that the reduction in surface NED becomes stronger with increasing distance from the impact point, i.e., the absorbing effect of the surface is cumulative as the distance increases. This decrease is probably dominated by the absorption of ions by the surface, as the spatially resolved reflection coefficient (not shown) and the spatial distribution of the NED (blue dashed line in Fig. 9(b)) have similar dependences on x.

Figure 10(a) illustrates that for normally-incident ions, the forward surface has a stronger effect on the 2D NED distribution than the backward surface, and that NED is not affected away from the surfaces, consistent with Fig. 8(a). Figures 10(b) and (c) confirm the former observation by showing lower values of the NED ratio $F_{2D}/F_{2D,\infty}$ at the forward surface (Fig. 10(c)) than at the backward surface (Fig. 10(b)). The NED ratio at the backward surface (Fig. 10(b)) deviates less dramatically from unity than at gracing incidence (Fig. 9(b)). Fig-

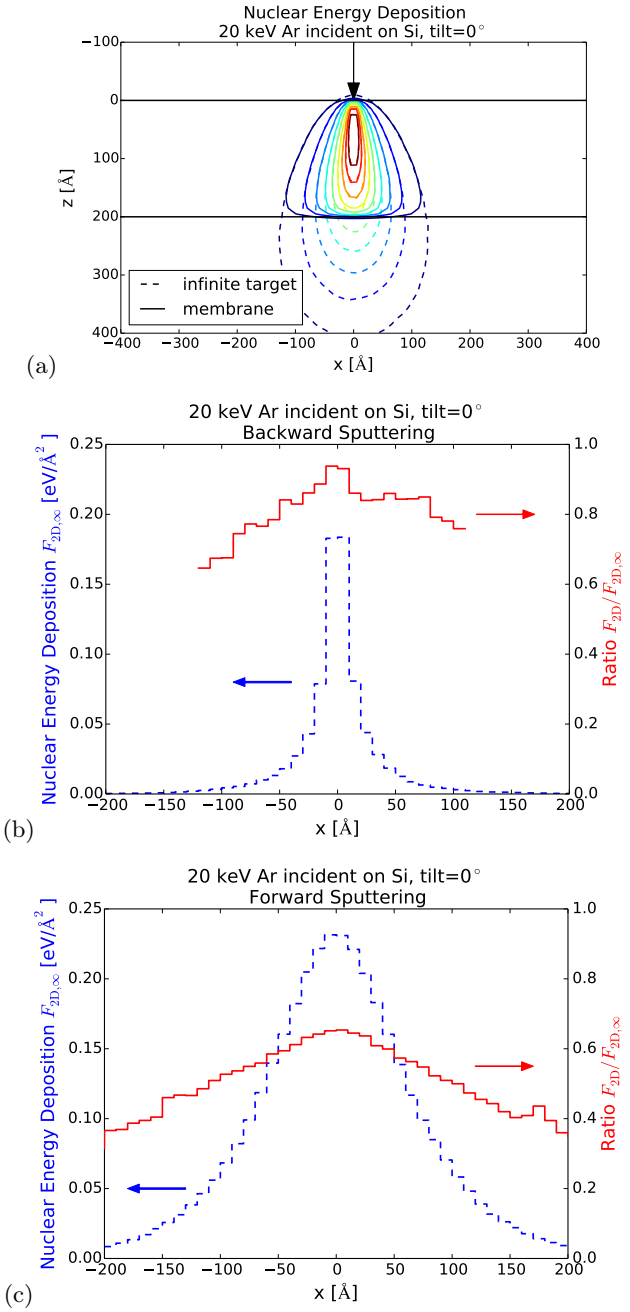

Figure 10: (a) 2D NED distributions for 20 keV Ar normally-incident on a 200 Å thick silicon membrane. This distribution is shown along the backward surface in (b), and along the forward surface in (c). For the interpretation of the line types see Fig. 9.

ures 10(b) and (c) also demonstrate that the ratio of the finite to the infinite medium NED decreases with increasing distance from the impact point for normally-incident ions on both the backward and forward surfaces.

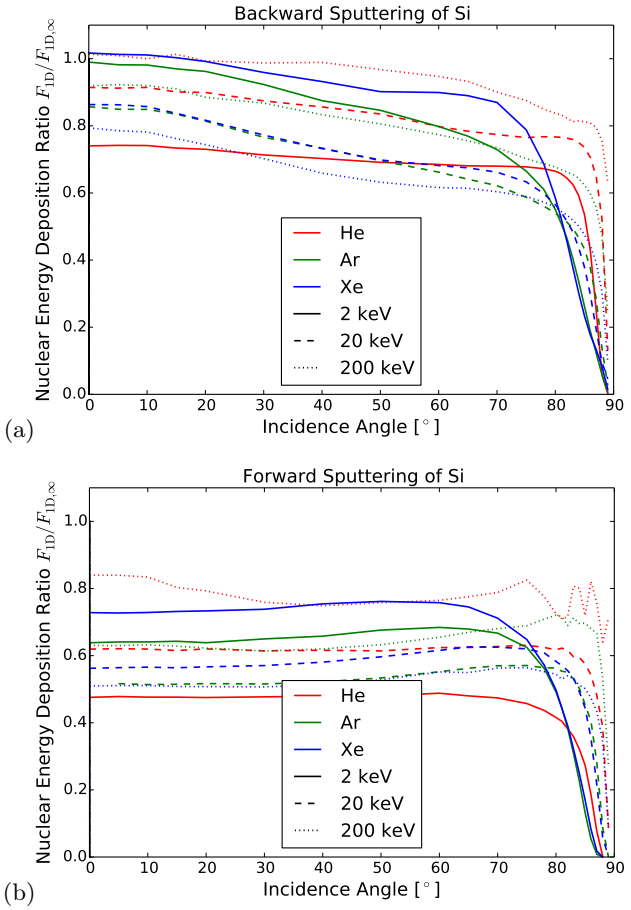

Figure 11: NED ratio $F_{1D}(z)/F_{1D,\infty}(z)$ (a) at the backward surface ($z = 0$) and (b) at the forward surface ($z = a$) as a function of incidence angle for He, Ar, and Xe ions with energies of 2, 20, and 200 keV.

B. Dependence on Ion Beam Parameters

To analyze how the influence of the surface on NED is affected by changing the ion beam parameters, we will use spatially unresolved data, as we did in Section III B. The NED ratio $F_{1D}(z)/F_{1D,\infty}(z)$ is shown as a function of the incidence angle at the backward surface ($z = 0$) and at the forward surface ($z = a$) in Figs. 11(a) and (b), respectively. In both cases the dependence is weak at angles that are not close to grazing incidence, and the NED ratio continuously decreases towards zero when the angle exceeds $70° - 80°$. These plots also show that the NED ratio is smaller for forward than for backward sputtering ($0.5 - 0.8$ versus $0.7 - 1.0$ at non-glancing angles). The reduced NED ratios near grazing incidence and for forward sputtering are consistent with Figs. 9 and 10, respectively; Fig. 11 shows that these are general trends.

The ion mass dependence of the NED ratio $F_{1D}/F_{1D,\infty}$ for normal incidence is shown in Fig. 12. The trends are not very clear except that the NED ratio is smaller for forward sputtering than for backward sputtering.

According to Sigmund's assumptions (i) and (ii), the

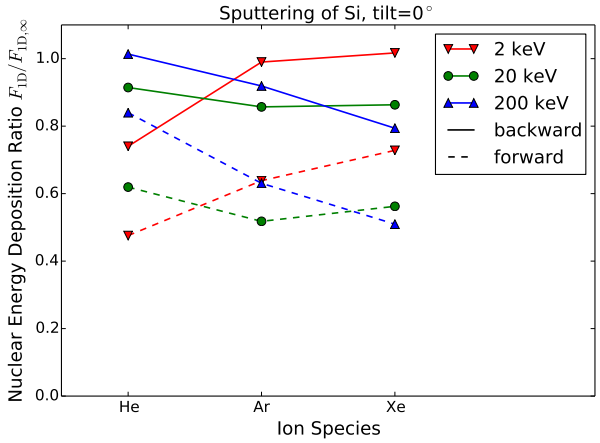

Figure 12: (a) Ion mass dependence of the NED ratio $F_{1D}(z)/F_{1D,\infty}(z)$ at the backward ($z = 0$) and forward surface ($z = a$) for normal incidence.

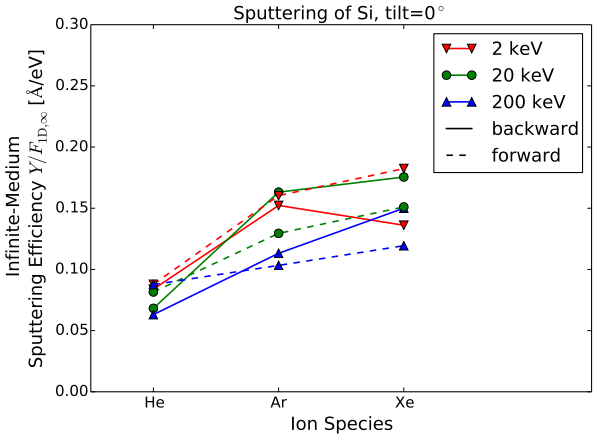

Figure 13: Ion mass dependence of the infinite-medium sputtering efficiency $Y/F_{1D,\infty}$ at normal incidence.

sputtering efficiency $\bar{\bar{\Lambda}} = Y/F_{1D}$ is a constant and the NED ratio $F_{1D}/F_{1D,\infty}$ is equal to one. We have seen that there are significant discrepancies between our simulation results and these assumptions. In light of the tendencies noted in the preceding paragraph, a natural question to ask is whether the errors inherent in Sigmund's assumptions (i) and (ii) cancel one another to some extent. To address this issue, we consider the product of the sputtering efficiency $\bar{\bar{\Lambda}}$ and the NED ratio $F_{1D}/F_{1D,\infty}$. This infinite-medium sputtering efficiency $\bar{\bar{\Lambda}}_\infty = Y/F_{1D,\infty}$ should be a constant if Sigmund's assumptions (i) and (ii) are valid; it is shown in Fig. 13 for normally-incident ions. Comparing to Figs. 5(a) and 12 it can be seen that there is still a pronounced ion mass dependence, but the dependencies on energy and forward versus backward sputtering are significantly reduced. Nevertheless, the minimum and maximum infinite-medium sputtering efficiencies (which are attained for 200 keV He backward sputtering and 2 keV Xe forward sputtering, respectively) still differ by a factor of 3. Within the more conventional range of beam parameters (Ar and Xe ions at 2 and 20 keV), however, the difference is reduced to a factor of 1.5. The partially compensating effects of the dependencies of sputtering efficiency and NED ratio are discussed further in the following subsection.

C. Discussion

In Section IV A, two mechanisms for NED reduction by the surfaces were discussed. The first one, backscattering of ions (Fig. 8(b)), reduces NED over the entire thickness of the membrane, although not to the extent expected if the backscattered ions had no effect at all on the NED. The second mechanism, the reduction in NED by the absorption of recoils generated by unreflected ions, is a higher-order effect: The recoils that produce NED in the $z > 0$ half-space in the infinite-medium but not in the finite-target simulation, either have crossed the plane $z = 0$ first in negative and then in positive z direction, or they have been generated in the $z < 0$ half-space by other recoils that have crossed the plane $z = 0$ in negative z direction before. These recoils are on average less energetic than the primary recoils generated by the reflected ions and therefore have a smaller range. This effect therefore primarily operates close to the surfaces, and leads to the short-range decays of NED as the surfaces are approached in Figs. 8(a) and 8(b).

Figures 9(b), 10(b), and 10(c) show that the NED ratio varies across the surface and decreases as a function of distance from the impact point. This indicates that the absorption of ions and recoils by the surface is a cumulative effect as the collision cascade develops away from the impact point. Similar dependencies of the NED ratio on the distance from the impact point are observed for normal and near-grazing incidence because the effects of ion backscattering and absorption of recoils by the surface are related: Close to glancing incidence, the reduction in NED is probably mainly due to the absorption of ions by the surface. At normal incidence, ion backscattering is negligible, but subcascades develop laterally from the center of the cascade ($x = 0$). These subcascades interact with the surface in a similar manner to the recoil cascades of near-grazing-incidence ions.

The effect of the backward surface on the NED distribution is stronger near grazing incidence (Figs. 8(b) and 9(b)) than at normal incidence (Figs. 8(a) and 10(b)). This may be explained by the fact that at grazing incidence the center of the collision cascade is situated quite close to the surface, and so larger subcascades may be "absorbed" by the surface than in the case of normal incidence. An analogous argument explains the larger reduction in NED at the forward surface than at the backward surface (Fig. 8(a)) for normal-incidence bombardment: The forward surface is close to the position of the NED maximum, and so larger and more energetic subcascades intersect that surface and are "ab-

sorbed" by it.

In Section IV B, we found that the dependencies of the sputtering efficiency and of the NED ratio on the ion mass and energy partially compensate when the two quantities are multiplied. A possible explanation for this is the following: More energetic recoils lead to a larger sputtering efficiency, since a larger fraction of the recoils is able to surmount the surface potential. At the same time, they result in a smaller NED ratio, since the surface has a greater effect on larger, more energetic subcascades. The compensation, however, is only partial, and compensation is not always observed for the spatial dependence of the sputtering efficiency and the NED ratio. For instance, the same trends for the forward sputtering efficiency and the NED ratio are observed for 20 keV Ar ions (Figs. 3(b) and 10(c)).

V. GAUSSIAN APPROXIMATION

A. Spatial Dependence

Sigmund's third assumption is that the NED distribution in an infinite medium can be approximated by a Gaussian with its maximum at $\zeta = a$ along the ion incidence direction, as given by Eq. (5). A Gaussian has zero skewness γ. For the skewness γ of the 1D infinite-medium NED distribution for 20 keV Ar, IMSIL yields the relatively moderate value $\gamma = 0.64$. In addition, Hofsäss and Bradley [27] reported NED densities that agree very well with Gaussians in both the longitudinal and lateral directions. However, the main problem with the Gaussian approximation is the neglect of the correlation between longitudinal and lateral NED distributions, as will be shown in the following.

In Fig. 14(a), the 2D NED distribution for 20 keV Ar in an infinite Si medium with the ions starting at the origin and initially moving parallel to the z axis is compared with the corresponding Gaussian approximation. For the latter, values of a and the longitudinal and lateral standard deviations α and β consistent with the MC simulations were used. At first sight, the distributions seem to agree well. However, closer inspection reveals a sharp peak in the MC results along the incident ions' initial path which is absent in the Gaussian approximation. This leads to a much narrower NED distribution along the plane $z = 0$ for the MC results than for the Gaussian approximation (see Fig. 14(b)). Thus, the Gaussian approximation predicts more nonlocal sputtering than the MC simulations give.

Correlations between longitudinal and lateral distributions can be characterized by the depth dependence of the lateral standard deviation measured in slices perpendicular to the ions' incidence direction. As can be seen from Fig. 14(c), the lateral standard deviation increases by a factor of three between $z = 0$ and $z = 600$ Å, a depth where NED is still appreciable. On the plane $z = 0$, its value is about half of its global value β, consistent with

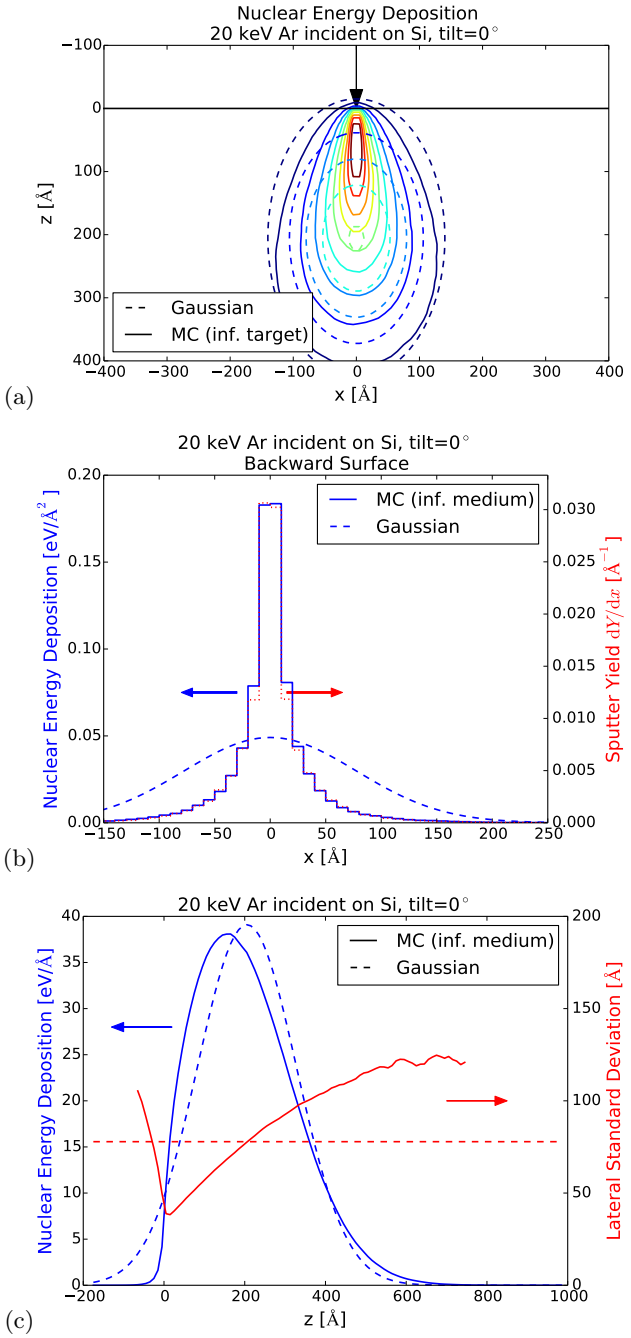

Figure 14: NED distributions obtained with MC **in an infinite medium** (solid lines) and with the Gaussian approximation (dashed lines) for 20 keV Ar for normal-incidence impact on the plane $z = 0$: (a) 2D distribution, (b) 1D distribution along the plane $z = 0$, and (c) depth distribution with depth-resolved lateral standard deviation. The color coding of the contour lines representing the 2D distribution in panel (a) is identical to that of Fig. 9(a). The red dotted line in panel (b) represents the spatially resolved sputter yield. The red dashed line in panel (c) indicates the global lateral standard deviation β.

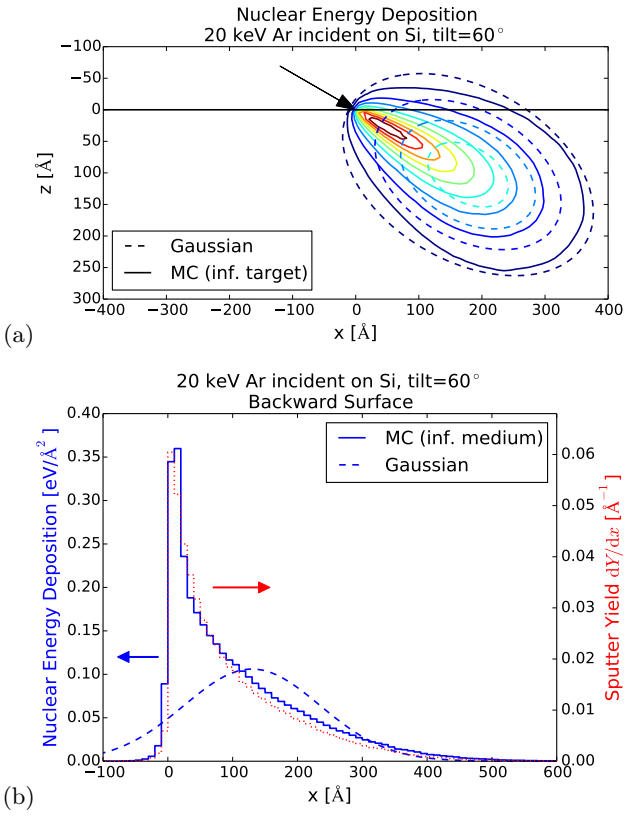

Figure 15: NED distributions obtained with MC **in an infinite medium** (solid lines) and with the Gaussian approximation (dashed lines) for 20 keV Ar at an incidence angle of 60°: (a) 2D distribution and (b) distribution along the surface. The color coding of the contour lines representing the 2D distribution in panel (a) is identical to that of Fig. 9(a). The red dotted line in panel (b) represents the spatially resolved sputter yield.

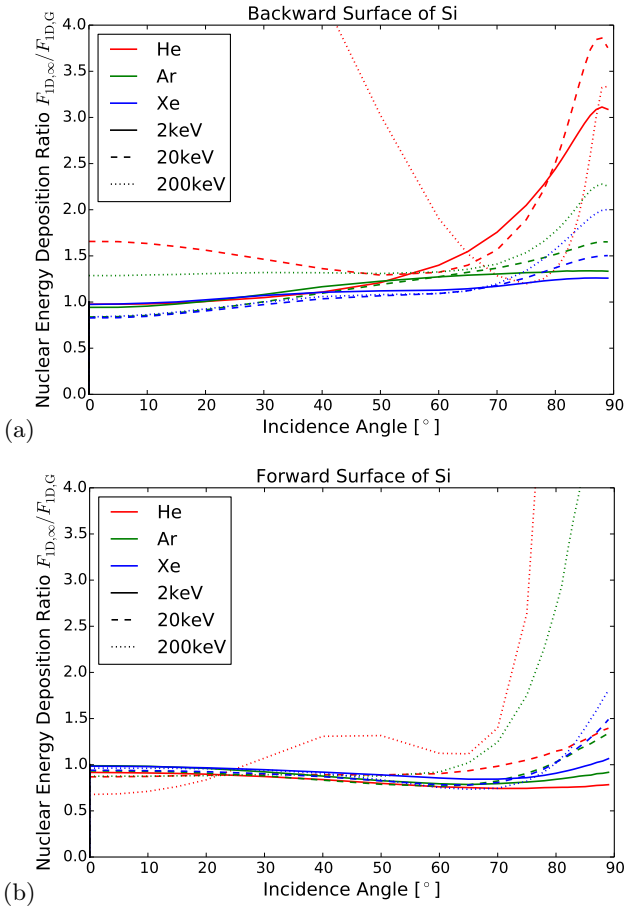

Figure 16: NED ratio $F_{1D,\infty}(z)/F_{1D,G}(z)$ (a) at the backward surface ($z = 0$) and (b) at the forward surface ($z = a$) as a function of incidence angle for He, Ar, and Xe ions with energies of 2, 20, and 200 keV.

the results of Fig. 14(b). The depth dependence of the lateral standard deviation is not taken into account by Sigmund's Gaussian approximation.

The deviation between the NED distribution and the Gaussian approximation is even more severe for oblique-incidence impacts on the plane $z = 0$. When the beam direction and thus the infinite-medium NED distribution is rotated with respect to the plane $z = 0$, the plane intersects the high NED concentration region close to the impact point, and so the NED distribution in the plane is peaked close to the point of impact (Fig. 15(b)). In contrast, the Gaussian approximation has its maximum at

$$\bar{x}_G = \frac{a \sin\theta}{\sin^2\theta + (\alpha/\beta)^2 \cos^2\theta}, \qquad (12)$$

which is larger than the distance of the NED peak from the impact point according to the MC simulations at oblique incidence. Fig. 15 demonstrates that near-grazing incidence is not required for this discrepancy to become significant: The incidence angle in the simulations of Fig. 15 is only 60°.

This is an important finding of our study. In applications, a Gaussian with fixed parameters a, α, and β – usually derived from infinite-medium calculations – is used to predict the NED at surfaces for oblique impact. Our results show that this can be a very poor approximation indeed.

B. Dependence on Ion Beam Parameters

In analogy with Fig. 11, we show in Fig. 16 the ratio of the approximated and the approximating NED density, which here is the ratio of the infinite-medium NED density $F_{1D,\infty}(z)$ and the Gaussian approximation $F_{1D,G}(z)$. This ratio is shown as a function of incidence angle for the backward surface ($z = 0$) and for the forward surface ($z = a$) in panels (a) and (b), respectively. For the two heavier ions (Ar and Xe) and incidence angles that are not too high, the ratio is close to unity, i.e., Sigmund's assumption (iii) does not introduce appreciable errors into the calculation of the total energy deposition at the surface and the total sputter yield. For **energetic** light ions

or incidence angles exceeding $70° - 80°$, the error is significant. **The former is to be expected since the large contribution of electronic stopping leads to non-Gaussian NED distributions.**

C. Discussion

The errors introduced by the Gaussian approximation mainly stem from the concentration of NED along the initial ion track (see Figs. 14(a) and 15(a)), which is caused by the fact that the majority of the incident ions only gradually change direction when penetrating into the target. The beam spreads out deeper into the target, which causes spreading of the NED distribution as well. This is characterized by an increase in the lateral standard deviation (Fig. 14(c)) and a decrease in the maximum NED density as we move along the ion incidence direction. Since Sigmund's Gaussian approximation uses an average lateral standard deviation, it usually overestimates the width of the NED distribution on the plane $z = 0$ (Figs. 14(b) and 15(b)).

VI. COMBINED EFFECT OF ALL ASSUMPTIONS

In the previous section we saw that the Gaussian approximation produces significant errors in the spatial distribution of the sputtered atoms. These errors are usually larger than those introduced by the non-constant sputtering efficiency and the influence of the surface (Figs. 3, 9, and 10). Figures 14(b) and 15(b) illustrate this since the spatial dependence of the sputter yield (red dotted histograms) is much closer to the NED distributions calculated by MC (blue solid histogram) than to the Gaussian approximation (blue dashed lines).

To provide an overview of the quality of the spatial dependence of the ejected atoms predicted by Sigmund's model, we show in Fig. 17 the ratio of the mean exit position of the sputtered atoms $\bar{x}_{\mathrm{d}Y/\mathrm{d}x}$ and the center of the Gaussian approximation $\bar{x}_{\mathrm{G}}$ as a function of incidence angle (Fig. 17(a)); the ratio of the corresponding standard deviations, $\sigma_{\mathrm{d}Y/\mathrm{d}x}$ and σ_{G} (Fig. 17(b)); and the skewness $\gamma_{\mathrm{d}Y/\mathrm{d}x}$ (Fig. 17(c)), where the skewness is defined as the mean value of $(x - \bar{x})^3/\sigma^3$. The dependencies of the first two moments largely follow those of the Gaussian approximation alone (not shown). Only at near-glancing angles is there a sharp decrease in the ratios that is not due to the Gaussian approximation. This decrease occurs because close to grazing incidence the sputtering efficiency is peaked close to the impact point (Fig. 3(d)) due to the effect illustrated in Fig. 7, and because the NED ratio $F_{\mathrm{2D}}/F_{\mathrm{2D},\infty}$ decreases as a function of distance from the impact point (Fig. 9(b)). At non-glancing angles the ratio $\bar{x}_{\mathrm{d}Y/\mathrm{d}x}/\bar{x}_{\mathrm{G}}$ generally decreases as a function of incidence angle. For commonly used beam parameters (Ar and Xe ions at 2 and 20 keV) and sufficiently oblique but non-grazing incidence, the ratio is within a relatively narrow band around and below unity. This is even more true for the ratio of the standard deviations which is between 0.8 and 0.9 for a wide range of angles. Including incidence angles close to perpendicular but not glancing

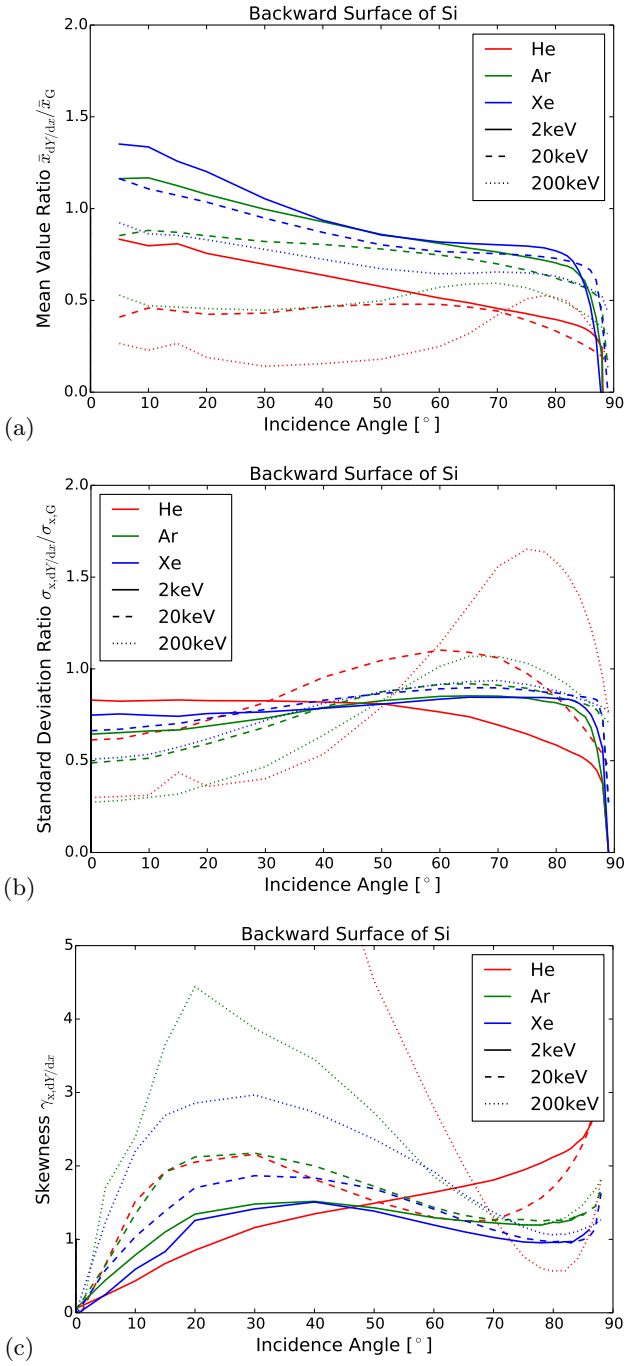

Figure 17: Ratios (a) of the mean values $\bar{x}_{\mathrm{d}Y/\mathrm{d}x}$ and $\bar{x}_{\mathrm{G}}$ and (b) of the standard deviations $\sigma_{\mathrm{x,d}Y/\mathrm{d}x}$ and $\sigma_{\mathrm{x,G}}$ of the sputtering distribution $\mathrm{d}Y/\mathrm{d}x(x)$ and the NED distribution $F_{\mathrm{2D,G}}(x, z = 0)$, and (c) the skewness of the sputtering distribution $\mathrm{d}Y/\mathrm{d}x(x)$ as a function of the incidence angle for He, Ar, and Xe ions with energies of 2, 20, and 200 keV.

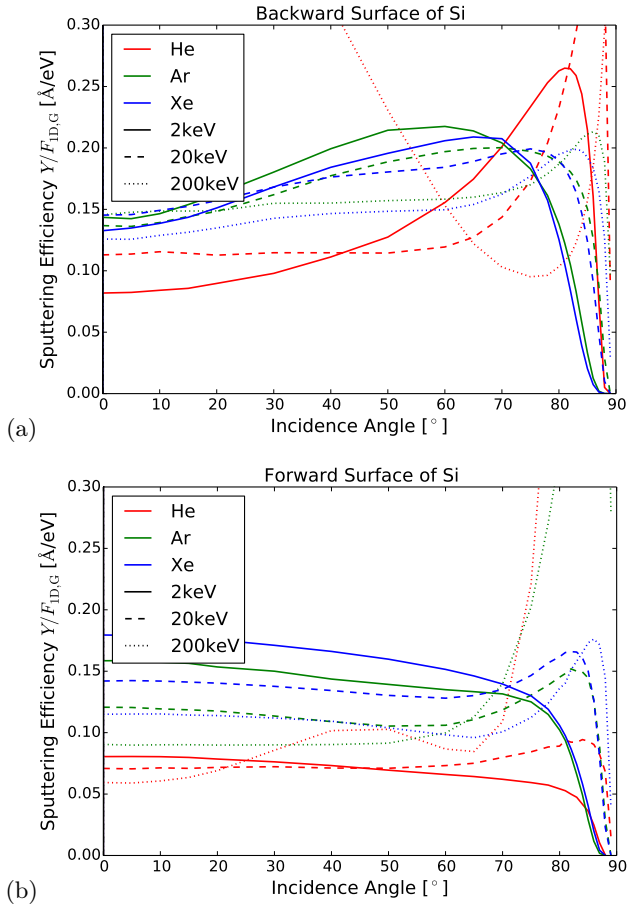

Figure 18: Effective sputtering efficiency $\bar{\bar{\Lambda}}_{\rm eff} = Y/F_{\rm 1D,G}(z)$ needed in Sigmund's model to obtain the correct sputter yield Y (a) at the backward surface ($z = 0$) and (b) at the forward surface ($z = a$) as functions of the incidence angle for He, Ar, and Xe ions with energies of 2, 20, and 200 keV.

conditions, the Sigmund model describes the first two moments of the spatial distribution of sputtered atoms within a factor of 2.

Figure 17(c) shows that skewnesses larger than unity occur for a wide range of incidence angles. **We note that the concentration of NED along a narrow elongated region in the direction of the incident ion, as described in connection with Fig. 15, drives the skewness in the positive direction. This effect is so strong that for energetic light ions it exceeds the negative skewness of the NED distributions that would show up in the spatial sputter yield distribution at large incidence angles if only assumptions (i) and (ii) were valid.** It may be concluded that the spatial distribution of sputtered atoms has a significant asymmetry except at incidence angles very close to normal. Since the Gaussian distribution has a skewness of zero, the Sigmund model is not able to describe this asymmetry.

In Section IV B, we saw that the errors in the spatially unresolved quantities incurred by making Sigmund's assumptions (i) and (ii) partially compensate for one another. It is natural to ask whether the errors in the spatially unresolved quantities made by adopting all three of Sigmund's assumptions compensate for each other to an even greater extent. To address this question, we computed the product of the MC sputtering efficiency $\bar{\bar{\Lambda}} = Y/F_{\rm 1D}$ (Fig. 4) and the NED ratios $F_{\rm 1D}/F_{\rm 1D,\infty}$ (Fig. 11) and $F_{\rm 1D,\infty}/F_{\rm 1D,G}$ (Fig. 16) at the backward and forward surfaces. In Figs. 18(a) and (b), the resulting effective sputtering efficiency

$$\bar{\bar{\Lambda}}_{\rm eff} = \frac{Y}{F_{\rm 1D,G}(z)} \tag{13}$$

is shown for $z = 0$ and $z = a$, respectively, as a function of incidence angle for He, Ar, and Xe ions with energies of 2, 20, and 200 keV. The NED distribution $F_{\rm 1D,G}(z)$ must be multiplied by this factor to obtain the MC sputter yield according to the Sigmund theory. $\bar{\bar{\Lambda}}_{\rm eff}$ was calculated by taking the ratio of the MC sputter yield and the total NED deposited at the surface in the Gaussian approximation using parameters a, α, β, and ε obtained from MC simulations. Any variation of $\bar{\bar{\Lambda}}_{\rm Sigmund}$ indicates a deficiency of Sigmund's model.

Comparing Figs. 4, 11, 16, and 18, it may be concluded that there are no significant compensating effects beyond the one discussed in Section IV B: The NED ratios $F_{\rm 1D,\infty}/F_{\rm 1D,G}$ (Fig. 16) are close to each other for the various commonly employed ion energies and masses, provided the angle of incidence is not too close to 90°. Their dependencies on the incidence angle are weaker than those of the sputtering efficiencies $\bar{\bar{\Lambda}}_{\rm eff}$ (Fig. 18) and in the same direction (they increase as a function of incidence angle for backward sputtering and decrease for forward sputtering). This means that Sigmund's assumption (iii) amplifies the trends produced by assumptions (i) and (ii). The pronounced angular dependencies of the NED ratios $F_{\rm 1D,\infty}/F_{\rm 1D,G}$ (Fig. 16) for He ions at the backward surface and 200 keV He and Ar ions at the forward surface are much stronger than the corresponding dependencies of the sputtering efficiency $\bar{\bar{\Lambda}}$ (Fig. 4) and the NED ratio $F_{\rm 1D}/F_{\rm 1D,\infty}$ (Fig. 11). The Gaussian approximation is therefore the cause of the strong dependence of the effective sputtering efficiency on incidence angle for these beam parameters (Fig. 18). At near-grazing incidence, the NED ratio $F_{\rm 1D,\infty}/F_{\rm 1D,G}$ (Fig. 16) increases as a function of incidence angle and therefore counteracts the dependencies due to assumptions (i) and (ii) to some extent. However, this effect is not strong enough to prevent the sharp decrease of the effective sputtering efficiency at high angles of incidence which results from assumptions (i) and (ii).

We close this section by summarizing the data presented in Figs. 18(a) and (b). The effective sputtering efficiency varies between 0.10 Å/eV and 0.22 Å/eV for Ar and Xe ions with energies of 2 and 20 keV and incidence angles up to 80°. He ions with energies of 2 or 20 keV have lower effective sputtering efficiencies at moderate incidence angles and a more pronounced dependence on

angle. High energies (200 keV) in combination with light ions (He, Ar) may result in an effective sputtering efficiency that has a strong angular dependence and that can assume large values.

VII. DISCUSSION

As mentioned in the Introduction, Hossain et al. [25] concluded from their MD simulations that Sigmund's assumption (i) is invalid. They showed that the sputter yield has a narrower spatial distribution than the surface NED distribution, consistent with a sputtering efficiency that decreases as a function of distance from the impact point. Qualitatively, we obtain the same result (Fig. 3(c)) at impact energies (2 keV) comparable to those investigated by Hossain et al. (250 eV and 1.5 keV). The difference between the spatial distributions of sputter yield and surface NED, however, diminishes or reverses sign as the impact energy is increased. Hossain et al. also found the peak of the sputter yield to be at the same position as the maximum of the NED distribution for all incidence angles. We find this to be approximately true for our 2 keV data (not shown), but not for higher energies and large incidence angles, as illustrated by the strong spatial dependence of the sputtering efficiency for a 20 keV He beam with $\theta = 80°$ (Fig. 3(d)).

Based on the results of their MD simulations, Hossain et al. came to the conclusion that Sigmund's assumption (iii) is a good approximation. This is contrary to the results we presented in Section V. At near-grazing incidence, the Gaussian approximation produces a maximum at a distance from the impact point that is approximately equal to a, while the maximum of the NED distribution and of the sputter yield distribution (Fig. 15) are much closer to the impact point. The difference again is more pronounced at higher energies, but is already significant at 2 keV in our data.

Bradley and Hofsäss [27, 44] observed an apparent additional rotation of the NED distribution when θ approaches glancing incidence in Hossain et al.'s results. They proposed a modification to Sigmund's model that rotates the NED distribution further than the ion beam when the incidence angle is increased. In this way a larger part of the NED distribution is moved out of the target, which tends to reduce surface NED at large incidence angles, and thus allows for the experimentally observed sputter yield maximum. The 2D NED distributions shown in Fig. 9(a) do not support this model. While the contour lines on the bulk side of the distribution might give the impression of a slight rotation towards the surface, it is clear that the main effect of the surface is localized in a shallow subsurface region, and therefore cannot be described by an additional rotation. This feature might not have shown up in Hossain et al.'s results because of limited spatial resolution. The slight apparent rotation within the bulk can equally well be described by a reduction in range measured from the impact point.

While Bradley and Hofsäss's modification of Sigmund's model correctly predicts a maximum of the sputter yield as a function of incidence angle, it generally does not yield a maximum of the spatially resolved sputter yield close to the impact point at oblique incidence. Instead, it usually predicts that the maximum appears close to a distance of a from the impact point. For example, with the parameters given in [27] the infinite-medium NED distribution of Fig. 9(a) should be rotated by $1.15 \times 85° = 97.75°$ in the modified Sigmund model to give the semi-infinite medium distribution. According to Eq. (12) the maximum of the surface NED would then be at $\bar{x}_G = 0.97\,a$ from the impact point, while the maximum of the MC distribution (Fig. 9(b)) is at $\bar{x} \approx 25\,\text{Å} \approx a/8$.

Our approach is based on Monte Carlo simulations of the energy deposition produced by ion irradiation. It has been shown that this type of simulation models the physics of linear collision cascades faithfully [33, 45]. So-called non-linear collision cascades or collision spikes, in which moving recoil atoms collide with other moving recoil atoms, are not modeled by our Monte Carlo code. However, the influence of collision spikes is most pronounced for heavy ions bombarding heavy target atoms [46] and is hence not pronounced for Si targets. In addition, we note that Sigmund's [5, 24] model is based on the concept of linear collision cascades. In his model, effects of target crystallinity – such as channeling of the incident ion or linear collision sequences of recoil atoms [47] – are neglected; this appears appropriate in our case of Si irradiation, since Si quickly amorphizes under ion irradiation.

Finally, we note that the results presented here have been obtained for an elemental target; for a compound target, the effects of irradiation are richer since sputtering is non-stoichiometric and, for prolonged bombardment, stoichiometry and surface morphology changes influence each other [14]. While simulating of processes of this kind is possible [48, 49], it is outside the scope of the present paper. Note that it is also known that in a compound target, energy deposition and hence the NED is non-stoichiometric [50].

VIII. CONCLUSIONS

In this paper, we used Monte Carlo simulations to test the validity of Sigmund's model of spatially resolved sputtering. For commonly employed ion beam parameters, i.e., for ions that have masses that are not too low, energies that are not too high, and angles of incidence that are not too close to grazing, the Sigmund model gives the sputter yield and the first two moments of its spatial distribution to within a factor of 2. The predictions of the Sigmund model can deviate even more substantially from the simulation results if the beam parameters are

unusual.

Sigmund's model is based on the three assumptions we discussed in Section I. Our Monte Carlo results demonstrate that all three of these assumptions can be poor approximations. **While it has previously been observed [27] that** the sputtering efficiency, which is the ratio of the sputter yield to the nuclear energy deposited, depends on the ion mass, energy and angle of incidence, **we have systematically studied and explained these dependencies here. We also showed that the sputtering efficiency varies** from point to point on the solid surface. Furthermore, the spatial distribution of the nuclear energy deposited is strongly affected by the proximity of the solid surface and is typically not close to being Gaussian.

The Gaussian approximation is the main source of error in the spatially resolved sputter yield, as it is not able to describe the significant, always positive skewness of the distribution along the projection of the beam direction onto the surface. This positive skewness is due to energy deposition in a narrow, elongated region around the undeflected ion direction that increasingly overlaps the surface as the incidence angle is increased. In contrast, the Gaussian approximation induces only moderate errors in the total sputter yield, except at large incidence angles where it partially counteracts the larger errors induced by the two other approximations. The Gaussian approximation also produces significant errors in the total sputter yield for light high-energy ions. This is not surprising, since the dominance of electronic stopping results in highly non-Gaussian range and damage profiles in this case. On the other hand, apart from the Gaussian approximation, the Sigmund theory does reasonably well even for the light He ion.

As expected, the surface causes a decrease in NED at large incidence angles due to ion reflection. The reduction in NED is caused by the fact that once the ions have been reflected they do not generate recoil cascades that would deposit energy if the medium were infinite. This has already been pointed out by Sigmund [28]. Surprisingly, we find that at low ion energies, the influence of ion reflection on the sputtering efficiency is equally important. We explain this by considering the large fraction of ions that do not penetrate into the target. These ions do deposit energy in the topmost layer of atoms, but they only generate recoils that move into the target. Conversely, we find that backward sputtering efficiencies increase with incidence angle at moderate angles. This is explained by direct sputtering of recoils by the incident ions. We also find that sputtering efficiencies increase with ion mass, which is due to the larger fraction of high-energy recoils produced by heavier ions. Finally, forward sputtering from a membrane is more efficient than backward sputtering due to a larger fraction of energetic recoils reaching the forward surface, but this effect is largely compensated for by a larger reduction in energy deposition near the forward surface than at the backward surface. These results have been obtained for membrane thicknesses equal to the mean depth of energy deposition. A complete investigation of the effect that varying the membrane thickness and incidence angle has on forward sputtering will be carried out in the future.

Given its deficiencies, it may seem surprising in retrospect that the Sigmund model has proven to be a useful starting point for theories of the nanoscale pattern formation that occurs when a solid surface is bombarded with a broad ion beam. However, it does capture some important features of ion sputtering. As in the Sigmund model, sputtering is a nonlocal effect: the maximum of the distribution of exit points of sputtered atoms is downstream from the ion's point of impact for oblique-incidence bombardment. In addition, to make a theory of the pattern formation, the dependence of the sputter yield on the surface curvature at the point of impact is needed [21]. Recent work has shown that even though the Sigmund model does not do particularly well in predicting the sputter yield of a flat surface, it does much better in describing how the sputter yield changes as the surface curvature is increased provided that the curvature is not too large [22, 23].

ACKNOWLEDGMENTS

We thank W. Möller from Helmholtz-Zentrum Dresden-Rossendorf for providing the TRI3DST data for Fig. 2, and H. Hofsäss from Universität Göttingen for discussing the differences between the IMSIL and SDTrimSP data given in Table I. R.M.B. would like to thank the National Science Foundation for its support through grant DMR-1305449.

[1] For example, see B. Ziberi, M. Cornejo, F. Frost, and B. Rauschenbach, J. Phys. Condens. Matter **21**, 224003 (2009).

[2] For a review, see J. Muñoz-García, L. Vázquez, M. Castro, R. Gago, A. Redondo-Cubero, A. Moreno-Barrado, and R. Cuerno, Mater. Sci. Eng. R **86**, 1 (2014).

[3] S. Facsko, T. Dekorsy, C. Koerdt, C. Trappe, H. Kurz, A. Vogt, and H. L. Hartnagel, Science **285**, 1551 (1999).

[4] F. Frost, A. Schindler, and F. Bigl, Phys. Rev. Lett. **85**, 4116 (2000).

[5] P. Sigmund, J. Mater. Sci. **8**, 1545 (1973).
[6] R. M. Bradley and J. M. E. Harper, J. Vac. Sci. Technol. A **6**, 2390 (1988).
[7] R. Cuerno and A.-L. Barabási, Phys. Rev. Lett. **74**, 4746 (1995).
[8] G. Carter and V. Vishnyakov, Phys. Rev. B **54**, 17647 (1996).
[9] M. A. Makeev and A.-L. Barabási, Appl. Phys. Lett. **71**, 2800 (1997).
[10] M. A. Makeev, R. Cuerno, and A.-L. Barabasi, Nucl. Instrum. Meth. Phys. Res. B **197**, 185 (2002).
[11] M. Castro, R. Cuerno, L. Vázquez, and R. Gago, Phys. Rev. Lett. **94**, 016102 (2005).
[12] B. Davidovitch, M. J. Aziz, and M. P. Brenner, Phys. Rev. B **76**, 205420 (2007).
[13] V. B. Shenoy, W. L. Chan, and E. Chason, Phys. Rev. Lett. **98**, 256101 (2007).
[14] R. M. Bradley and P. D. Shipman, Phys. Rev. Lett. **105**, 145501 (2010).
[15] M. Moseler, P. Gumbsch, C. Casiraghi, A. C. Ferrari, and J. Robertson, Science **309**, 1545 (2005).
[16] C. S. Madi, E. Anzenberg, K. F. Ludwig, and M. J. Aziz, Phys. Rev. Lett. **106**, 066101 (2011).
[17] M. Castro and R. Cuerno, Appl. Surf. Sci. **258**, 4171 (2012).
[18] M. Castro, R. Gago, L. Vázquez, J. Muñoz-García, and R. Cuerno, Phys. Rev. B **86**, 214107 (2012).
[19] S. A. Norris, M. P. Brenner, and M. J. Aziz, J. Phys. Condens. Matter **21**, 224017 (2009).
[20] S. A. Norris, J. Samela, L. Bukonte, M. Backman, F. Djurabekova, K. Nordlund, C. S. Madi, M. P. Brenner, and M. J. Aziz, Nature Commun. **2**, 276 (2011).
[21] M. P. Harrison and R. M. Bradley, Phys. Rev. B **89**, 245401 (2014).
[22] M. L. Nietiadi and H. M. Urbassek, Appl. Phys. Lett. **103**, 113108 (2013).
[23] H. M. Urbassek, R. M. Bradley, M. L. Nietiadi, and W. Möller, Phys. Rev. B **91**, 165418 (2015).
[24] P. Sigmund, Phys. Rev. **187**, 768 (1969).
[25] M. Z. Hossain, J. B. Freund, and H. T. Johnson, J. Appl. Phys. **111**, 103513 (2012).
[26] J. Ziegler, *SRIM - The Stopping and Range of Ions in Matter* (IIT, 2015).
[27] H. Hofsäss and R. M. Bradley, J. Appl. Phys. **117**, 174310 (2015).
[28] P. Sigmund, in *Sputtering by Particle Bombardment I*, edited by R. Behrisch (Springer, Berlin, 1981), pp. 9–71.
[29] M. D. J. Bowyer, D. G. Ashworth, and R. Oven, J. Phys. **D 29**, 1286 (1996).
[30] P. F. A. Alkemade, in *Nanofabrication: Techniques and Principles* (Springer, 2014), pp. 275–300.
[31] G. Hobler, Nucl. Instrum. Meth. Phys. Res. B **96**, 155 (1995).
[32] C. Ebm and G. Hobler, Nucl. Instrum. Meth. Phys. Res. B **267**, 2987 (2009).
[33] W. Eckstein, *Computer Simulation of Ion-Solid Interactions* (Springer, Berlin, 1991).
[34] A. Desalvo and R. Rosa, Radiat. Eff. **31**, 41 (1976).
[35] J. P. Biersack, Nucl. Instrum. Meth. Phys. Res. B **27**, 21 (1987).
[36] G. Hobler and A. Simionescu, Nucl. Instrum. Meth. Phys. Res. B **102**, 24 (1995).
[37] S. Lindsey and G. Hobler, Nucl. Instrum. Meth. Phys. Res. B **303**, 142 (2013).
[38] M. L. Nietiadi, L. Sandoval, H. M. Urbassek, and W. Möller, Phys. Rev. B **90**, 045417 (2014).
[39] J. F. Ziegler, *SRIM-2013*, URL `http://www.srim.org`.
[40] L. D. Landau and E. M. Lifshits, *Mechanics* (Pergamon, New York, 1960).
[41] H. M. Urbassek and M. Vicanek, Phys. Rev. B **37**, 7256 (1988).
[42] M. W. Sckerl, M. Vicanek, and P. Sigmund, Nucl. Instrum. Meth. Phys. Res. B **102**, 86 (1995).
[43] M. W. Sckerl, P. Sigmund, and M. Vicanek, Mat.-Fys. Medd. Dan. Vid. Selsk. **44** (1996), no. 3.
[44] R. M. Bradley and H. Hofsäss, J. Appl. Phys. **116**, 234304 (2014).
[45] W. Eckstein and H. M. Urbassek, in *Sputtering by Particle Bombardment*, edited by R. Behrisch and W. Eckstein (Springer, Berlin, 2007), vol. 110 of *Topics Appl. Physics*, pp. 21–31.
[46] P. Sigmund, Appl. Phys. Lett. **25**, 169 (1974), erratum: ibid. **27**, 52 (1975).
[47] M. T. Robinson, in *Sputtering by Particle Bombardment I*, edited by R. Behrisch (Springer, Berlin, 1981), p. 73.
[48] M. S. Bharathi, H. Ramanarayan, and Y. W. Zhang, Appl. Phys. Lett. **99**, 083103 (2011).
[49] W. Möller, Nucl. Instrum. Meth. Phys. Res. B **322**, 23 (2014).
[50] M. Vicanek, U. Conrad, and H. M. Urbassek, Phys. Rev. B **47**, 617 (1993).
[51] Eq. (4) follows from Eq. (2.3.26) of Ref. [28] using $Y = \Lambda F$.